ISSN 0001-4338, Izvestiya, Atmospheric and Oceanic Physics, 2009, Vol. 45, No. 3, pp. 357–371. © Pleiades Publishing, Ltd., 2009.
Original Russian Text © N.G. Yakovlev, 2009, published in Izvestiya AN. Fizika Atmosfery i Okeana, 2009, Vol. 45, No. 3, pp. 383–398.

Reproduction of the Large-Scale State of Water and Sea Ice in the Arctic Ocean in 1948–2002: Part I. Numerical Model

N. G. Yakovlev

Institute of Numerical Mathematics, Russian Academy of Sciences, ul. Gubkina 8, Moscow, 119333 Russia
e-mail: iakovlev@inm.ras.ru

Received January 29, 2008; in final form, October 14, 2008

Abstract—This paper completes a series of studies conducted with a numerical model of low spatial resolution for the area of the North Atlantic and Arctic Ocean north of 65° N without including Hudson Bay to reproduce the monthly mean state in 1948–2002. The paper gives a detailed description of the physical formulation of the problem, the approximations and parametrizations that were employed, and the parameters of atmospheric and oceanic external forcings. Generally, the author follows the requirements of the protocol of the Arctic Ocean Model Intercomparison Project (AOMIP). The paper analyzes the main monthly mean characteristics: ice thickness, ice-drift velocity, snow thickness, velocity of currents, and temperature and salinity, which were derived as multiyear averages over 1958–2002. A good reproduction of the following sea-ice characteristics is noted: ice thickness, propagation area, ice concentration, and drift velocity. For example, the annual mean ice-drift velocity is about 3.33 cm/s, which is consistent with the data obtained from drifting buoys, which yield an annual mean ice-drift velocity of 3.65 cm/s. At the same time, there are problems of reproducing the observed snow-thickness distribution. The use of parametrizations of horizontal turbulence of the Neptune-Effect type and eddy transfer for a scalar makes it possible to conserve the cyclonic circulation in the Atlantic water layer although the low spatial resolution gives no way of explicitly reproducing the narrow topographic jet. In conclusion, we briefly discuss the main unsolved problems and, primarily, the problem of reproducing the freshwater content. The model and further versions of it will be used in the European Commission project DAMOCLES (Developing Arctic Modeling and Observing Capabilities for Long-Term Environmental Studies) to assess the sensitivity of the Arctic Ocean to the parameters of external forcing and to evaluate the role of tides in the formation of the Arctic Ocean's climate.

DOI: 10.1134/S0001433809030098

1. INTRODUCTION

This paper completes a series of studies conducted with a numerical model of low spatial resolution for a small area of the world ocean north of 65° N without including Hudson Bay. The main problem formulated in the early period of this model (1997–1998) was to construct algorithms and to test different parametrizations. During the author's involvement in the Arctic Ocean Model Intercomparison Project (AOMIP) [1] (the official site of this program can be found at http://fish.cims.nyu.edu/project_aomip/overview.html) since 2002, the model has been significantly improved and brought up to date. Profound experience has been accumulated in formulating problems for the Arctic Ocean dynamics and interpreting of the final results with allowance for the emerging measurement data and fresh calculation results with different models of the highest level.

Currently, the scientific community agrees that the Earth's polar areas are poorly known in all of their aspects and, at the same time, are potentially the most prone to global climate changes. Some uncertainty in views on the role of polar areas in climate change and on the possible response of the Arctic to these changes made it necessary to establish such a major program as the International Polar Year 2007–2008 (IPY 07–08). This program includes a number of national and international projects; for example, the integrated European contribution to IPY 07–08 named DAMOCLES (the official site of this project can be found at http://www.damocles-eu.org.) Special emphasis in this project is placed on the development of numerical models as an instrument for processing heterogeneous measurement data and on the monitoring of the states of the Arctic climate system to integrate the theoretical and empirical knowledge and, finally, to predict possible climate changes. The model presented in this paper and further versions of it will be used in the DAMOCLES project to assess the sensitivity of the Arctic Ocean to external forcing parameters and evaluate the role of tides in Arctic Ocean climate formation.

2. MODEL DOMAIN, CHOICE OF COORDINATE SYSTEM, SYSTEM OF EQUATIONS, AND BOUNDARY CONDITIONS OF THE MODEL

Model Domain

We consider the area of the North Atlantic and Arctic Ocean north of 65° N without including Hudson Bay. Five islands are considered. The Canadian Archipelago is not described in detail. As a whole, the configuration of the model domain is close to that used by the author in [2–6], except that the Fram Strait shelves near Spitsbergen were slightly deepened and a small shelf near the Norwegian coast was produced for a more adequate description of alongshore jets, which are extremely important in this problem. In addition, the Canadian Archipelago includes three straits: Nares, McClure, and a model strait near Prince Patrick Island. The Bering Strait is assumed to be open. Eight major rivers with their estuaries regarded as straits of special type are taken into account. The White Sea, which cannot be described with reasonable accuracy under the given spatial resolution, is taken as an estuary of the Severnaya Dvina River.

In this model, the equations of ocean and sea-ice dynamics are written in the widely used coordinate system of a "spherical layer" (λ, θ, z) (longitude, complement of latitude to 90°, and depth taken vertically downward from the ocean surface in a state of rest with respect to the Earth) with its poles located at points with geographical coordinates of 180° E, 0° N ("North" Pole) and 0° E, 0° N ("South" Pole). All of the terms in the equations are invariant with respect to the choice of pole positions, except for the Coriolis force. The spatial resolution of the model is 1° in horizontal variables in the rotated system of coordinates (i.e., around 111.2 km). There are also 16 unequally spaced vertical layers in the z system of coordinates with crowding near the ocean bottom.

Ocean Dynamics and Thermodynamics

We use the Boussinesq, hydrostatic, and seawater incompressibility approximations, which have become traditional in investigations of the large-scale ocean dynamics (the so-called "primitive" system of equations). Following the Boussinesq hypothesis, we write the operators of momentum turbulent exchange and the operators of heat/salts diffusion in a simple form, assuming that the turbulent stress tensor is diagonal and the horizontal turbulent-exchange processes are isotropic. In general, the formulation of the problem of ocean dynamics (the equations and boundary conditions) follows the works of the author [2–5]. In view of this, we will note the differences between the model presented here and the versions used earlier.

The new model incorporates all metric terms in the advection and turbulent viscosity operators for the components of velocity of ocean currents and ice drift. Although the contribution of these components to the balance of momentum is relatively small for the coordinate system with a model pole away from the given domain, these terms become important for conserving angular momentum in integrating the problem for a time period of about 100 years.

The equations of the ocean model are written for a domain with a flat (in the coordinates of a spherical layer) upper surface; for oscillations of the level, a linearized kinematic condition is used. The pressure at the upper oceanic surface is produced by atmospheric pressure and by the pressure produced by oscillations of the ocean level and by the weight of ice with its snow cover.

For the flux of solar radiation penetrating into the water area, an exponential decay formula is used. Under the assumption of clarity of Arctic waters, we have $\zeta_1 = 120$ cm for the shortwave band of the spectrum, $\zeta_2 = 28$ m for the longwave band, and $R_1 = 0.68$ for the fraction of shortwave radiation as proposed in [7]. Let us note immediately that the assumption of clarity may be incorrect for some areas (for example, summer estuaries with a rise in admixtures and plankton blooming).

The vertical turbulent exchange in the high latitudes can be successfully parametrized with a relatively simple scheme based on the Monin–Obukhov formula [8, 9] and with a choice of parameters similar to [10, 11]; thus, unstable stratification leads to increased vertical turbulent exchange coefficients. The bottom boundary layer is not described explicitly. To make the problem regular, we place the lower and upper limits to the range of the vertical turbulent viscosity coefficient: $10 \le \nu \le 10^5$ cm^2 s^{-1}. The coefficients of vertical turbulent diffusion of heat and salts are proportional to the vertical turbulent viscosity coefficient and $\nu_T = \nu_S = 10^{-2}\nu$, respectively. The additional limitations $0.1 \le \nu_T$, $\nu_S \le 10^3$ cm^2 s^{-1} are also imposed. It is important that, in most cases, the model operates in the lower limit $\nu_T = \nu_S = 0.01$ for stable stratification. Some additional diffusion appears during numerical implementation, which, to some extent, replaces the physical turbulent diffusion.

To parametrize the alongshore jets, we use the results of studies [12–14]. The description of these jets is important in reproducing the heat and salt fluxes for the Atlantic water transport into the Central Arctic, which plays a significant role in the formation of the observed ocean climate. In [12], a simple parametrization based on the concept of a "statistically equilibrium" barotropic stream function is used, which describes the ocean state in the absence of large-scale external forcing:

$$\psi_N = lR_N^2 H. \tag{1}$$

Here, H is the ocean depth and the length scale $R_N \approx 3$–12 km according to numerous estimates (see, for example, [15]). The flow velocity corresponding to the stream function ψ_N is denoted as u_N.

This theory has been further developed in [13], where the equation of the time-average barotropic vorticity $\bar{\omega}$ was obtained under the hypothesis of a maximum rate of growth in entropy:

$$\frac{\partial\bar{\omega}}{\partial t} + J(\psi, \bar{q}) = A_E\nabla^2\bar{\omega} + \frac{A_E}{\mu}(\bar{\omega}^* - \bar{\omega}). \qquad (2)$$

Here, we use the original notation of the cited study: $\bar{\psi}$ is the stream function of the time-average current, $\bar{q}$ is the time-average potential vortex, $\bar{\omega}^*$ is the equilibrium vorticity related to the mean current defined in (1), and A_E is the horizontal turbulent exchange coefficient. The parameter μ is chosen from the condition that the energy and enstrophy conservation laws hold. It is important that, here, the resulting operator has the form of parametrization of an additional force ("topographic stress"), which leads to the formation of a jet stream over the features of the bottom topography. A comparison with the results of [4], where the same technique was used to simulate the Arctic Ocean, allows us to suggest that the parameter in the last term has the form $\frac{A_E}{\mu} = \vartheta \times A_E\ R_N^{-2}$, where $\vartheta = O(10^{-3})$. In the given model, we use the parameters $R_N = 5$ km and $\vartheta = 5 \times 10^{-3}$.

The above parametrization describes the generation of average current over the topography features, while the parametrization in [16] describes the effect of transfer of a scalar (temperature or salinity) by eddies generated on inclined isopycnic surfaces. Normally, the eddy transfer is used together with the parametrization of diffusion on isopycnic surfaces in the approximation that their angles of slope are small [17]. The given model includes no mixing on isopycnic surfaces to avoid the doubling of this effect by a similar mechanism arising from numerical implementation of the scheme of transfer with additional artificial downstream diffusion. The eddy transfer is simulated in terms of a "skew flux" with an antisymmetric tensor of turbulent diffusion coefficients [18]. The coefficient of "eddy diffusion" was assumed to be constant: $A_{gm} = 5 \times 10^6$ cm^2 s^{-1}; in addition, the coefficients of the eddy diffusion tensor were limited so that the slope of isopycnic surfaces was no more than 4×10^{-3} [19]. The slope of isopycnic surfaces was also limited in the upper mixing layer in line with [20].

Ice Thermodynamics

Generally, the model of local one-dimensional ice thermodynamics is based on the concepts described in [21] and is almost the same as the model used by the author in [3]. The thermodynamic module is applied to each of the 14 gradations of ice according to thickness: 0 (open water), 10, 20, 30, 50, 70 cm, 1, 1.5, 2, 3, 4, 5, 6, 10, and more than 10 m. The main difference from the previous version of the model is the parametrizations of albedo, heat flux from the ocean, radiation fluxes, and evolutionary changes in the ice concentration.

The thermodynamic model has the evident deficiency of disregarding the following parameters: the heat capacity of ice, the dependence of heat capacity and heat conductance on temperature and salinity of ice, and the distribution of ice salinity in its thickness. In view of this, the model has essentially a single vertical level for snow and two levels for ice. The use of the simplified thermodynamic model is justified by estimates indicating that the realistic description of ice dynamics is more important than the choice of a large number of vertical levels [22].

In the given model, the choice of albedo parametrization is similar to the CCSM2 sea-ice module in the climate model of the National Center for Atmospheric Research (Boulder, Colorado, United States) [23] with some simplifications associated with the fact that the integral albedo averaged over all wavelengths and angles of incidence is used, rather than a distinction being made between albedos in different spectral intervals (the corresponding approximate formula can also be found in [23]). By the term "wet" snow or ice, we mean a surface with a temperature higher than –1°C (this temperature initiates the formation of pools on the surface of snow or ice). Relatively thin snow lies in the form of the so-called "tails" and its effective albedo is calculated with allowance for the fraction of radiation penetrating into the open ice. The albedo values are given in the table.

The shortwave radiation penetrating into snow-free ice is parametrized by assuming that the portion of radiation not reflected from the surface is absorbed in the uppermost layer of ice [21]. This leads to a change in the effective albedo of ice, and the expression for the shortwave radiation flux involves an additional multiplier $(1 - i_0)$, where i_0 is the fraction of radiation penetrating into ice. According to observations, i_0 depends on the spectral composition of the incident radiation. This dependence can be regarded as a function of the cloud amount N [24] (cloudiness shifts the spectrum of solar radiation into the longwave range, thus increasing i_0): $i_0 = 0.18 + 0.17 \cdot N$. The radiation penetrating into ice attenuates exponentially with a length scale of $h_R = 1.5$ m [25], independent of wavelength. In this case, to conserve the two-layer approximation of the temperature profile in the ice column, the radiation penetrating into the ice is assumed to have no effect on its temperature. The radiation that passes through the ice is absorbed in the below-ice water layer in accordance with the exponential attenuation law for two gradations of radiation by wavelength.

Parametrization of snow and ice albedos depending on the surface temperature T, ice thickness h_i, and snow thickness depth h_s

Surface	Dry $T < -1°C$	Wet $T > -1°C$
α_s, snow	0.8	$\alpha_s = 0.8 - 0.1(T + 1)$
α_i, ice thickness h_i	$\alpha_i = \alpha_w + h_i(0.65 - \alpha_w)/50$, if $h_i \le 50$ cm, $\alpha_i = 0.65$, if $h_i > 50$ cm	$\alpha_i = \alpha_w + (0.65 - 0.075(T + 1) - \alpha_w)\, h_i/50$, if $h_i \le 50$ cm, $\alpha_i = 0.65 - 0.075(T + 1)$, if $h_i > 50$ cm
α_w, water	0.1	
Effective albedo of snow with thickness h_s, lying in the form of tails	$\alpha = s_f\,\alpha_s + (1 - s_f)(\alpha_i + (1 - \alpha_i)i_0)$, $s_f = \dfrac{h_s}{h_s + 2\text{ см}}$	

Note: i_0 is a parameter describing the fraction of radiation penetrating into ice and is assumed to depend on the cloud amount (see in text)

It is reasonable to suppose that the sensitive heat flux from ocean to ice Q_B is proportional to the difference between the temperatures of the ocean and lower surface of ice (equal to freezing temperature of seawater $T_F(S)$ [26]) and to the friction velocity at the water–ice interface $u_* = \sqrt{C_D}|(u - u_1)|/\sqrt{\rho_0}$ [27]:

$$Q_B = \rho_0 C_p\, St \cdot u_*(T(z = 0) - T_F(S)). \qquad (3)$$

where C_h is the heat capacity of water. The proportionality coefficient St (the Stanton number) varies in the range $St = 5.0 - 6.0 \times 10^{-3}$ [28]. In the model, it is $St = 5.5 \times 10^{-3}$. The coefficient C_D is calculated as a friction coefficient in the logarithmic profile of flow near a rough wall. According to measurement data, the roughness parameter [28] for the ice thickness characteristic of the Arctic is $z_0^* = 5$ mm, and the distance to the wall is taken to be $\delta z = 1$ m. In the given model, the roughness z_0 of the lower surface of ice is specified similarly to [22, 29] as a function of its thickness $h_i : z_0 = z_0^* \dfrac{h_i}{H_0}$, where it is assumed that $H_0 = 3$ m for the conditions of the Arctic Ocean. If it is supposed that the friction velocity is taken from the solution of the problem of combined ice and ocean dynamics, and consequently, the ocean current velocities are calculated at a distance of about a few meters from the interface, it is useful to introduce the lower and upper limits, for example, as $0.075 \le u_* \le 100$ cm/s.

Frazil ice (newly formed ice in open water) is generated if $T \le T_F(S)$. Generally, the model can generate frazil ice at any depth down to the bottom. In the generation of frazil ice, it is assumed that the melting heat of ice with saline pockets constitutes 0.92 of the melting heat of homogenous ice [30].

Newly formed ice is assumed to occupy open water and the area taken by the ice of the first gradation of thickness if its thickness is smaller than the upper limit of the second gradation of ice. Otherwise, the mass of frazil ice is distributed by ice gradations proportional to their concentration. The choice of a technique for the distribution of newly formed ice by gradations is important for parametrizing the rate of ice formation and the rate of convection caused by discharge of salt from ice into the ocean. In the present model, it is assumed that the thickness of frazil ice is 1 cm.

The changes in the mass of ice and snow and concentration of ice are calculated separately for each gradation of ice by its thickness. It is assumed that the change in the concentration of ice that is due to its lateral melting is proportional to the change in the thickness of ice due to its melting on the lower surface with a proportionality coefficient of 5×10^{-5} cm^{-1} (see the review of parametrizations in [23]).

The ice mass is redistributed by thickness gradations as a result of melting and freezing processes and ice hummocking during its motion. The latter process is described similarly to that proposed in [31–33].

When the ice mass is redistributed by thickness gradations, it is necessary to ensure that the heat content (in this case, the temperature of the ice surface) is conserved. In addition, it is necessary to ensure that the mass of snow located on ice is conserved. It was assumed that, with hummocking, half of the snow mass remains on the hummocking ice and the other half goes into water, producing the corresponding freshwater flow. During ice melting and freezing on the lower surface, the snow does not enter the water (except in the case of complete ice melting). Because the ice salinity is assumed to be constant through its thickness, the ice-salt mass is conserved automatically.

Ice Drift

The calculation of sea-ice drift velocity is based on [31–35]. We use an elastic–viscous–plastic rheology [35, 36], which is currently some kind of a standard in global and regional climate models. Here, the sea-ice "elasticity" is introduced as a technique allowing the problem of calculation of the stress-tensor components to be reduced formally to an evolutionary formulation and, thus, its numerical solution to be simplified.

A key difference from the standard formulation is that the balance of forces acting on ice includes the effect of atmospheric pressure and the additional pressure produced by the above-ice snow. In addition, unlike [34], it was not supposed that it is possible to disregard the inertial terms $m(\mathbf{u}_i \cdot \mathbf{\nabla})\mathbf{u}_i \approx 0$ for sea ice. Indeed, the calculations show that, near the Greenland coast, the instantaneous velocity of ice drift is no greater than 1 m/s; thus, for a spatial resolution as small as tens of kilometers, the advection becomes comparable to the Coriolis force. The balance of forces includes all metric terms emerging when the equations are written in the coordinate system of a spherical layer.

The friction coefficient at the air–ice interface for thick (more than 3 m) ice is calculated by a quadratic aerodynamic formula with a friction coefficient $C_w = 2.75 \times 10^{-3}$, which is consistent with the estimates obtained from observational data and model calculations [37]. Thin ice is assumed to be indistinguishable from water; therefore, in the range of medium-thickness ice from 0 to 3 m, a linear interpolation is taken for the coefficients of wind friction of water (according to [38]) and thick ice. Careful choice of the wind friction coefficient is important for reproducing the balance between the ice-formation rate and its transfer through the Fram Strait into the Norwegian–Greenland Sea. As noted above, the friction coefficient C_D at the water–ice interface is calculated as the friction coefficient in the logarithmic profile of flow at the rough wall by taking into account the change in the roughness parameter depending on the average ice thickness. The parametrization of friction at the water–ice interface implies, in accordance with the AOMIP protocol, that the angle between the velocity of ice drift and flow velocity in the upper layer is zero. Note also that the problem of parametrization of the friction coefficients for ice-drift calculations is discussed in [39].

The pressure in ice (or ice strength) is calculated on the basis of [31–33]. It is this type of parametrization that has recently found ever increasing use because, in spite of its somewhat greater complexity, this parametrization reproduces the ice-drift velocity more realistically for areas covered by thick (more than 3 m) ice [22, 40]. The parameters used for describing the hummocking process are the same as in [31, 32].

The boundary conditions on the "solid" shore and estuaries are set as no-slip conditions, and the ice-drift velocity at "liquid" boundaries is calculated under the assumption that the "radiation conditions" are applicable.

The interaction between the ocean and ice occurs through friction stress, heat flux, and freshwater flow.

Numerical Scheme

The numerical scheme for the ocean model is generally similar to the scheme proposed by the author in [3, 5]: it involves a method of spatial approximation on the basis of the finite element method, basic principles for solving the problem of ocean dynamics with an implicit-in-time description of the external gravitation mode, and reduction of the model to solution of the equations for the ocean level. However, there are also substantial differences. First and foremost, this concerns the modification of the advection scheme and the implementation of the ice-drift module and the boundary conditions within open boundaries.

As previously, the transfer of scalars (temperature and salinity) is calculated using numerical diffusion, which acts along the flow and partially replaces the actual large-scale turbulent diffusion [41–43]. Unlike its previous versions, the model uses stabilization with respect to all three spatial coordinates. To suppress the excessive dispersivity of the scheme, this version of the model does not use the "mass concentration method" for approximating the derivative with respect to time. The mass matrix is inverted by the method of successive upper relaxation. Because the actual problem always involves a good first approximation taken from the previous time step, the method converges usually in five to ten iterations. Since the use of efficient stabilization of the numerical solution and the suppression of artificial oscillations are of key importance, special emphasis will be placed on this.

The parametrization of the eddy transfer of a scalar does not substantially change the numerical scheme. The eddy transfer is treated separately in the time splitting scheme; this can be done because the corresponding operator is skew-symmetric. It can be easily found that, for recommended values of the eddy-transfer coefficients of no more than 10^8 cm^2 s^{-1}, the limitation on the time step in the explicit scheme remains unchanged and is determined by the usual transfer. The same is true for numerical downstream diffusion. The terms responsible for eddy transfer are approximated in time in the same manner as the normal transfer by using a predictor–corrector scheme.

To simplify the numerical algorithm, the ocean and ice modules were separated from each other: first, the ice-drift velocity was found with a linearized quadratic friction at the water–ice interface at each time step, and then the problem linearized at each time step for flow velocities was solved. This leads to a certain violation in the momentum conservation law in the water–ice system, which, however, can be due to inaccuracy in specifying ice rheology and turbulent viscosity of the ocean. In any case, this approach is used in all state-of-the-art ocean climate models. Like in previous versions, the problem of vertical turbulent exchange of momentum was treated at a separate splitting step and solved by an implicit method. The dynamics of sea ice is calculated by an explicit–implicit scheme, where the Coriolis force and friction on water are calculated implicitly. This helps the solution remain stable. Due to its nonlinearity, the rheology is approximated in time by the explicit Euler scheme, and the problem of sea-ice dynamics is solved using an internal cycle with a time step of 60 s. This approach can be regarded as the solution of the nonlinear problem of ice dynamics by simple iteration.

In contrast to the scheme for temperature and salinity, the scheme for transfer of sea-ice and snow characteristics includes artificial diffusion, which is calculated from the projection of the transfer rate onto the solution gradient, rather than from the transfer rate [42]; this makes the scheme less dissipative and retains strong numerical diffusion only in areas with steep gradients of the solution. Unfortunately, the use of artificial diffusion for transfer of sea-ice and snow characteristics (unlike for temperature and salinity) has no physical meaning. As in the case of temperature and salinity, the mass matrix is not diagonalized in the derivative with respect to time.

At the open boundaries of the model domain, different variants of radiation conditions are implemented that generally differ in the choice of the phase velocity of the signal. For temperature and salinity, the use of the radiation condition is based on the ideas of [44], with calculation of the phase velocity by solution gradients in the neighborhood of the boundary, generalized to the three-dimensional case. The phase velocity of transfer of sea-ice scalar characteristics was specified by the velocity at the node nearest to the boundary. The ice-drift velocity was calculated in the same way as temperature and salinity.

3. EXTERNAL FORCING

As a whole, the forcing parameters agree with the AOMIP requirements and were obtained by the author during his participation in this program. The high-frequency atmospheric forcing is specified by near-water daily average temperature and atmospheric pressure (NCEP/NCEP reanalysis data [45, 46]). The model is integrated in time using linear interpolation, assuming that the daily average values are reduced to the noon of a corresponding day.

The shortwave radiation (with allowance for the daily variation) is calculated by formulas [47] with a correction for cloudiness [21]. The total longwave radiation is calculated by widespread formulas [48].

The fluxes of sensible and latent heat were calculated by the conventional “aerodynamic” formulas with coefficients $C_H = 1.2 \times 10^{-3}$ and $C_L = 1.5 \times 10^{-3}$, respectively, for a stable boundary layer, and $C_H = C_L = 1.8 \times 10^{-3}$ for an unstable boundary layer (according to measurement data over water openings [49]; see also [25]). The stability of the boundary layer was determined in the model from the temperatures of air and the underlying surface.

The wind flow and tangent stress on water were calculated by bulk formulas on the basis of pressure data [38].

The relative humidity in the entire domain is assumed to be 90%. The pressure of saturated vapors was calculated by formulas [50]. In calculating the vapor pressure near the surface, we take into account the state of this surface (water or snow/ice). Over saline water, the saturation vapor pressure decreased by 2%. The pressure of saturated vapors in the atmosphere was assumed to depend on its temperature T_a; pressure over freshwater was taken for $T_a > 0$°C; otherwise, pressure over ice was taken.

The monthly average field of cloudiness was taken from atmospheric forcing data for the Ocean Model Intercomparison Project (OMIP) [51]. Note that there are large discrepancies between these data and Soviet/Russian data [52, 53], especially in September over the Barents Sea.

The average multiyear monthly mean precipitation was provided by M. Serreze to the participants of the AOMIP. This version [54] includes data obtained from stationary towers on the continent and islands and from drifting stations [55]. A comparison of precipitation data with other databases and atlases indicated [52, 53, 56] that the precipitation intensity was overestimated by 30%. In view of this, some correction was used in the calculations. The melting of snow that fell in winter on coastal areas of Norway and Spitsbergen and the related freshwater flow into the ocean in summer were disregarded.

In the straits, the radiation conditions for temperature and salinity are implemented [44]. Here, the temperature and salinity data from [57] are used. A spatial resolution of about 100 km does not allow the Canadian Archipelago straits to be considered in detail; therefore, the model includes three major straits: Nares, McClure, and a model strait near Prince Patrick Island, where the total net water flow from the Arctic into the North Atlantic is equally concentrated (2.4 Sv) [58]. The flows through the straits are assumed to be homogeneous in the section of straits and constant in time. A major difficulty in the regional formulation of the problem is the extended open boundaries with the Atlantic Ocean, through which considerable water, salt, and heat exchange occur. The flow on the Iceland–Norway section was taken to be constant: 8 Sv. Much observational data indicate that the spatial distribution of flow velocity is characterized by relatively high velocities in the upper 50-m layer, and the flow is nestled close to the continental slope.

Thus, the spatial structure is described using the following pattern for the flow velocity at the boundary:

$$u_b(\lambda, z) = \begin{cases} a(5 + lR_N^2 u_N), & z \le 50 \text{ m}, \\ alR_N^2 u_N, & z > 50 \text{ m}. \end{cases}$$

The positive direction corresponds to the flow into the Arctic Ocean (the units of all quantities are cm/s). The coefficient a is chosen so that the total flow is 8 Sv. The quantities u_N and R_N are, respectively, the flow velocity and the length scalefrom the parametrization of horizontal turbulent exchange (the "Neptune effect", see above). The flow through the Danish Strait was assumed to be 6.4 Sv plus an approximate difference between precipitation and evaporation of about 0.1 Sv (found a posteriori in the course of preliminary calculations). The profile of velocity was chosen to be linear in the strait width with a maximum on the Greenland shore and with a zero on the Iceland shore; in the vertical, the velocity in the upper 100-m layer is five times greater than the velocity in deeper layers. The Bering Strait is assumed to be open, with a given flow (0.8 Sv), which is considered to be constant in time, homogeneous in the strait section, and directed from the Bering Strait to the Arctic Ocean.

The model rivers are regarded as special-type straits without ice drift and heat and salt fluxes but with mass fluxes. The model takes into account seven major Eurasian rivers (Yenisei, Ob', Lena, Severnaya Dvina, Mezen, Pechora, and Kolyma) and the MacKenzie River in Alaska. The river flow was assumed to be homogeneous for the entire depth of the ocean, which distinguishes this model from the approximation frequently used in large-scale models that rivers can flow into the uppermost oceanic layer alone. The flow of each ith river was given by the formula $W_i = \alpha_i R(t)$, where α_i is the total annual flow of a given river and the function $R(t)$ is the same for all rivers. For simplicity, it was supposed that $R(t)$ is a piecewise constant function, which gives a monthly mean contribution to the total annual flow. The total annual flow of all rivers is estimated at 77872.2 m^3/s. If the flow not measured by the towers located on large rivers, which is estimated by some experts at 30% of the measured value, is taken into account, this estimate will be 101233.9 m^3/year or 3192.5 km^3/year (see [59], which is also very consistent with [60]). One of the problems is to balance the river flow by flows through straits; for simplicity, the model assumes that the river flow is instantaneously compensated by flows through the straits of the Canadian Archipelago, equally through the Nares and McClure straits and through the model strait in the area of Prince Patrick Island.

Because all modern data are unbalanced by freshwater flows, the salinity is specified by a climatic source on a time scale of relaxation to the climate on the ocean surface of 180 days [57]. This additional flow makes it possible to decrease the model trend in reproducing the freshwater content; the choice of this time scale has been confirmed by successful numerical experiments, including those conducted within the AOMIP.

4. CALCULATION RESULTS: AVERAGE MULTIYEAR MONTHLY MEAN CHARACTERISTICS

Organization of Calculations

The initial conditions were specified as zero flow velocities and a zero ocean level; the ice thickness was assumed to be 2 m if the ocean surface temperature was no higher than the freezing temperature, and the ice concentration was taken to be 0.9. The initial snow thickness was constant over the entire area covered by ice and equal to 10 cm. The temperatures of snow and the upper surface of ice were specified at –1°C. The model was integrated with a time step of 2 h (test calculations indicated smaller integration steps may change the solution only slightly). In the course of calculations, the monthly mean fields were kept for further analysis. Furthermore, additional data on the instantaneous flow and ice-drift velocities and on changes in temperature and salinity were kept, and the average ocean level was controlled to estimate the error in reproducing the balance of the water volume.

A detailed discussion of the calculation results will be presented in subsequent papers of the series. Here, we reproduce the average multiyear annual course of such quantities as the ice concentration and thickness, ocean level, flow velocities, and water salinity and temperature. The averaging period was from 1958 to 2002, and the first ten years of integration were eliminated because the adjustment of the parameters of ice and of the upper one-kilometer ocean layer and their attainment of a model quasi-equilibrium mode occurred in these years.

Sea-Ice and Snow Parameters

The resulting climatic distributions of the average ice thickness are shown in Fig. 1. The dashed line in the figures indicates the ice edge according to [61]. One can notice a good agreement between observational data and modeling results in the winter months. In summer, the model ice edge is located extremely far northward on the Siberian shelf. A possible explanation for this is the structure of the field of cloudiness and the assumption of water clarity. The experiments performed with the given model and the results of other models that can be found in the literature indicate that the ice is highly sensitive to cloudiness specification. The author believes that the use of more realistic data instead of those employed here makes it possible to change the position of the ice edge. The horizontal structure and absolute values of the ice

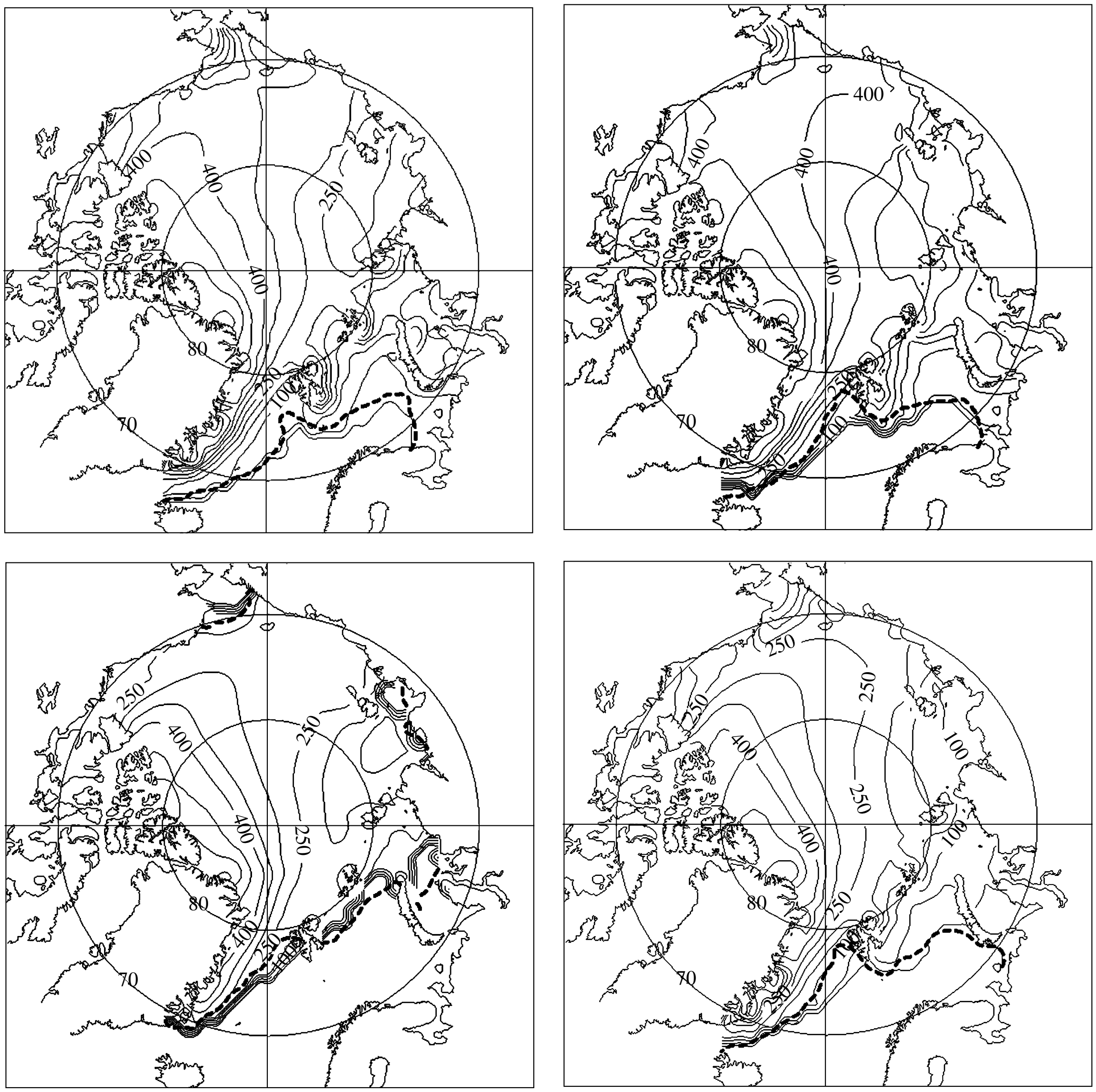

Fig. 1. Average ice thickness (cm). Left to right and bottom to top: February, May, August, and November. The dashed line indicates the ice edge as revealed by observations.

thickness are close to observational data and the results of calculations with state-of-the-art models [37, 40, 62]. Note the impact of ice drift on the formation of the structure of ice thickness: the ice is nestled close to the Canadian Archipelago and the northern shore of Greenland.

In the structure of ice-drift velocity (Fig. 2), one can clearly see an anticyclonic gyre centered at the northern end of the East Siberian Sea and the Transpolar transport in winter months. The multiyear monthly mean ice-drift velocity averaged over the water area constitutes 5.09 cm/s in December and slightly more than 1.3 cm/s in August. The maximum instantaneous velocity of ice drift can reach 1 m/s near the Greenland coast. The average ice-drift velocity during the year is approximately 3.33 cm/s. These results are generally consistent with data obtained with drifting buoys, which yield an annual mean ice-drift velocity of 3.65 cm/s [37, 63]. The small drift velocities in summer months are due to a weak and variable wind; in specific months, the drift velocity can be significantly higher. Note that the somewhat underestimated result is also caused by the low spatial resolution of the model and by the no-slip condition for ice on the coastal contour.

An analysis of the results on the reproduced ice cover shows that the model currently yields more realistic results than a previous version [3], with rheology of the "cavitating liquid" type and without calculation of the ice strength according to [31, 32].

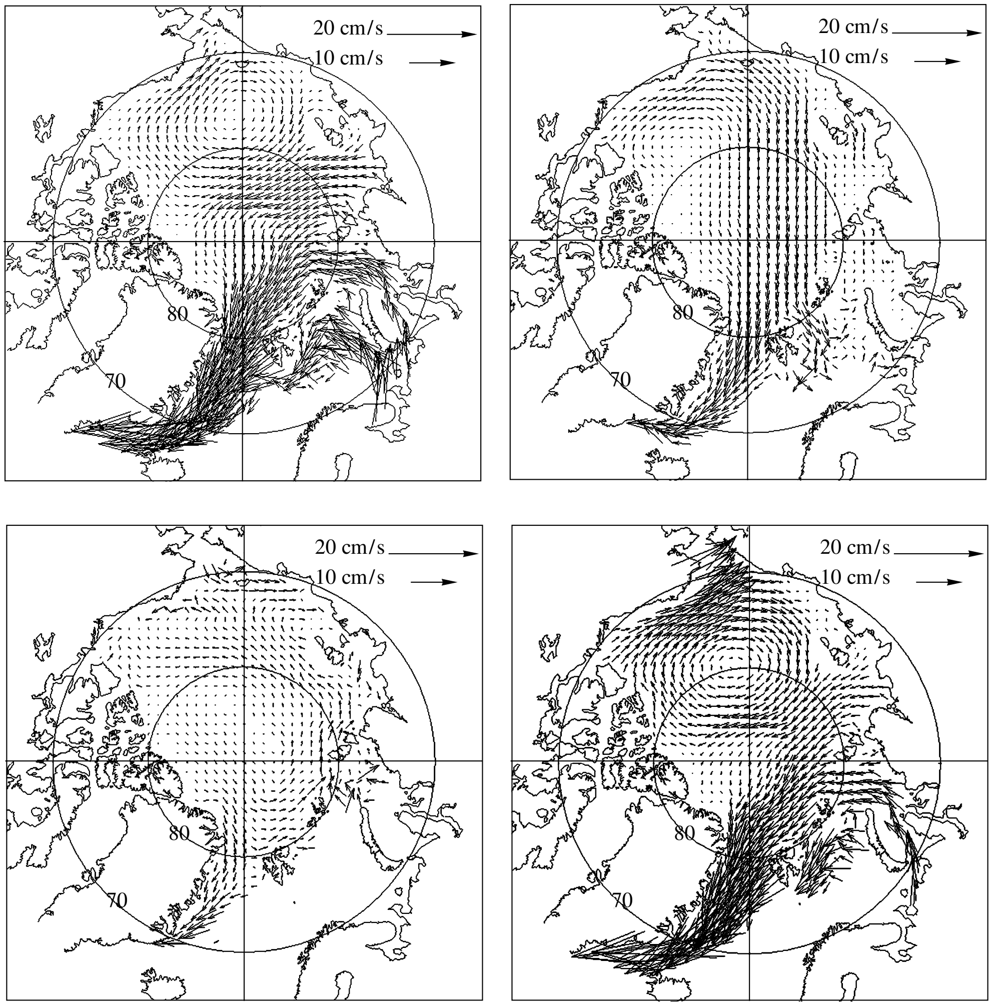

Fig. 2. Ice-drift velocity (the reference values are shown in upper right of the figure). Left to right and top to bottom: February, May, August, and November.

The snow-cover thickness is shown in Fig. 3 (in August, the snow completely disappears). Apparently, this structure of snow thickness is generally controlled by the given precipitation with the transport of moist air from the Atlantic and Pacific. Because the snow completely disappears in summer, no impact of ice drift is observed. For the reproduction of snow thickness, the specification of cloudiness is also of great importance. It should be accepted that these results are well consistent with data in [64], which may point to both the problem of specifying the precipitation and cloudiness over the Arctic Ocean and the problem of treating spatially sparse observational data on the thickness of snow cover. We did not manage to reproduce the increase of snow thickness toward the Canadian Archipelago and Greenland; the snow cover itself on the main water area of the Arctic Ocean is also approximately 1.5 times lower than the value given in [64]. In this case, in April, near the Greenland shore, the snow thickness reaches 45 cm, which is comparable to measurement data.

Flow Velocity

In the main volume of the ocean, the monthly mean climatic fields of flow velocity are subjected to minor changes during the year, which is generally confirmed by other calculations as well (see the results on the AOMIP site at http://fish.cims.nyu.edu/project_aomip/overview.html). The most noticeable changes are observed on the ocean surface and on the Siberian shelf under the action of wind and river flow. Let us consider the November velocities as an example (Fig. 4). Among the main structures in the surface flow velocity are the Transpolar transport, relatively strong flows in the Barents and Kara seas, and strong flows near the Bering Strait (Fig. 4a). This structure is fully consistent with the current views on the character of the Arctic Ocean circulation. The characteristic velocity of flows is about

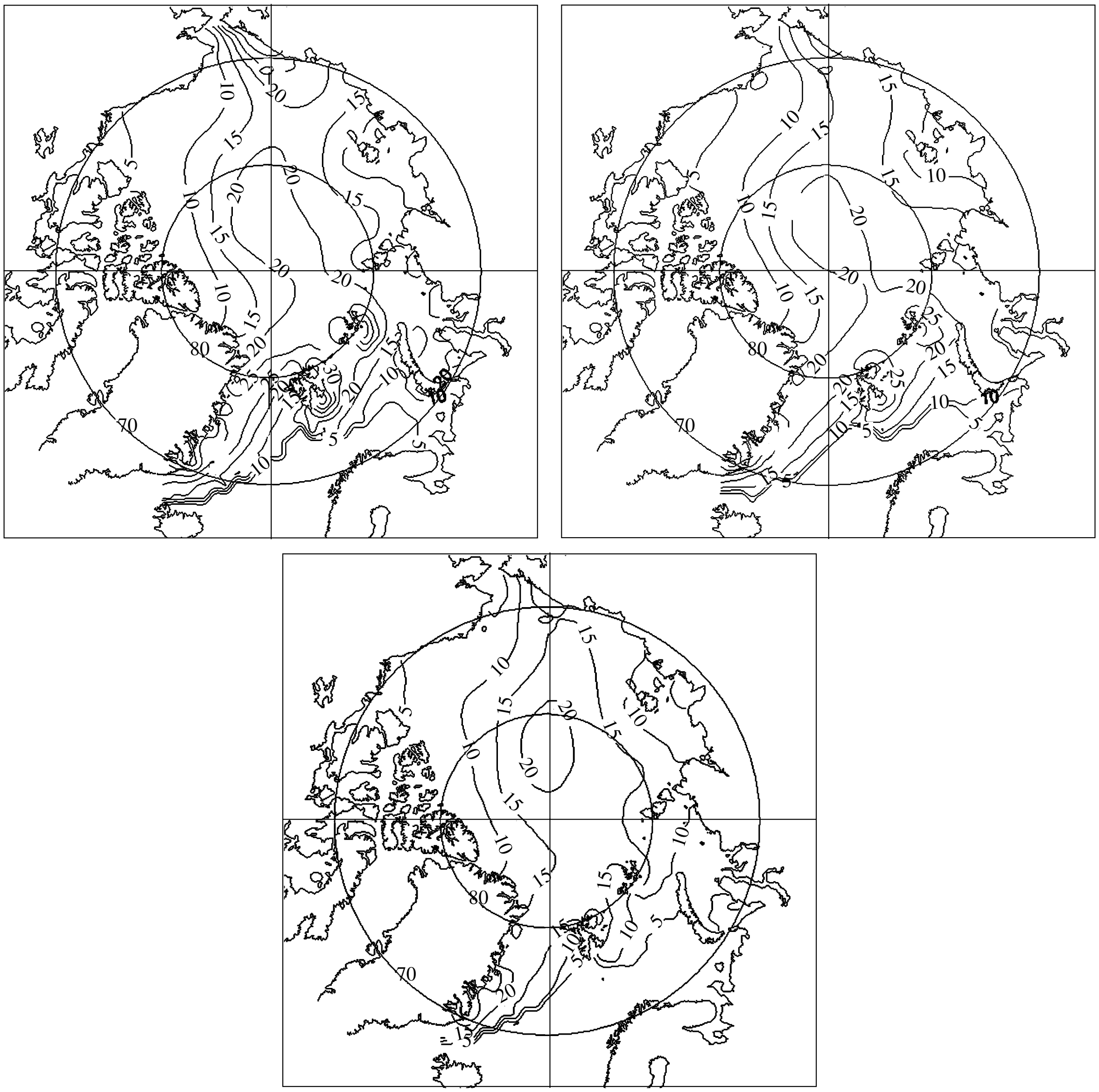

Fig. 3. Ice thickness (cm): February, May, and November. In August, the ice disappears completely.

3 cm/s at the ocean surface, about 20 cm/s on the Greenland shore, and about 1 cm/s in the Atlantic water layer at depths of 250–500 m. The structure of flow fields at a depth of 400 m (Fig. 4b) seems also quite realistic: one can see the reproduction of the set of flows in the Fram Strait and a cyclonic water circulation along the continental slope. In the Fram Strait at depths of 300–500 m, one can see a north-to-south cyclone; its western and eastern periphery can be identified with the East Greenland Current (EGC) and West Spitsbergen Current (WSC), respectively; the northern periphery is at the Franz Josef Land, and the southern periphery is at around 75° N. This cyclone can also be regarded as a combination of the EGC and WSC recirculations.

Most of these features were reproduced by the model even earlier; however, the previous versions were unable to support the cyclonic circulation in the Atlantic water layer during 55 years: normally, this circulation failed after 30 years in the model integration. The cyclonic circulation was supported with the help of parametrizations of horizontal mixing over varying bottom topography and eddy transfer of a scalar. A new feature is the appearance of a small anticyclone in the vicinity of the McClure Strait, which is likely to be due to an inconsistency between the boundary conditions for the salinity and flow velocity in this area.

(a)

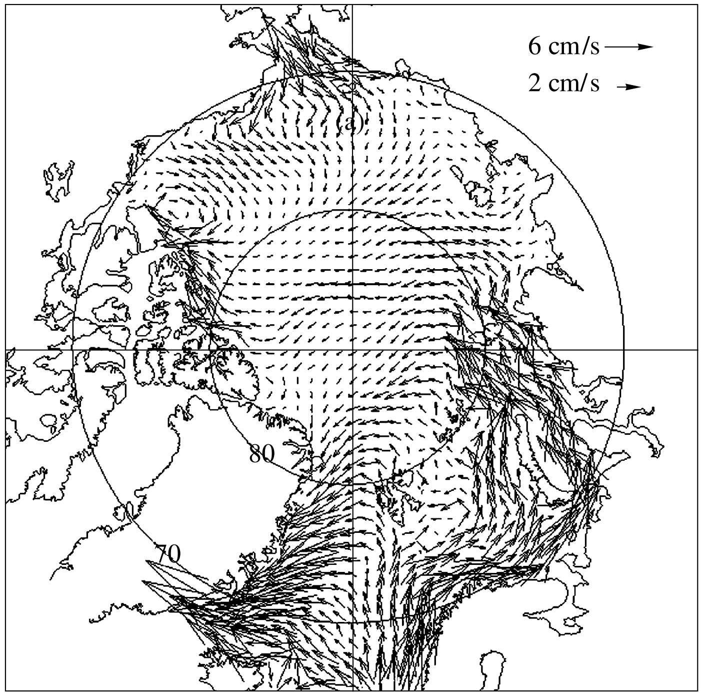

(b)

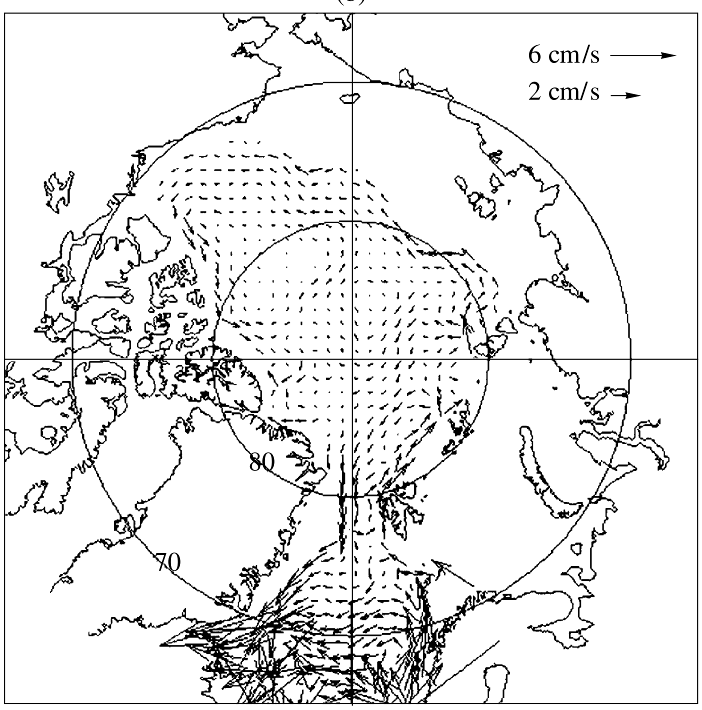

Fig. 4. Ocean current velocities (a) at the surface and (b) at the level of 400 m in November (the reference values are shown at the top right of the figure).

Temperature and Salinity

The horizontal distribution of temperature at depths of 50 and 400 m (the temperature for February is given) and surface salinity are shown in Figs. 5 and 6. At the ocean surface, the structure of the temperature field is apparently determined by the position of the ice edge; in the below-ice mixing layer with a depth of about 30 m, the spatial variation of temperature is small and the temperature is close to the freezing point. At a depth of 50 m (see Fig. 5a), the impact of ice is slightly deteriorated and one can notice the

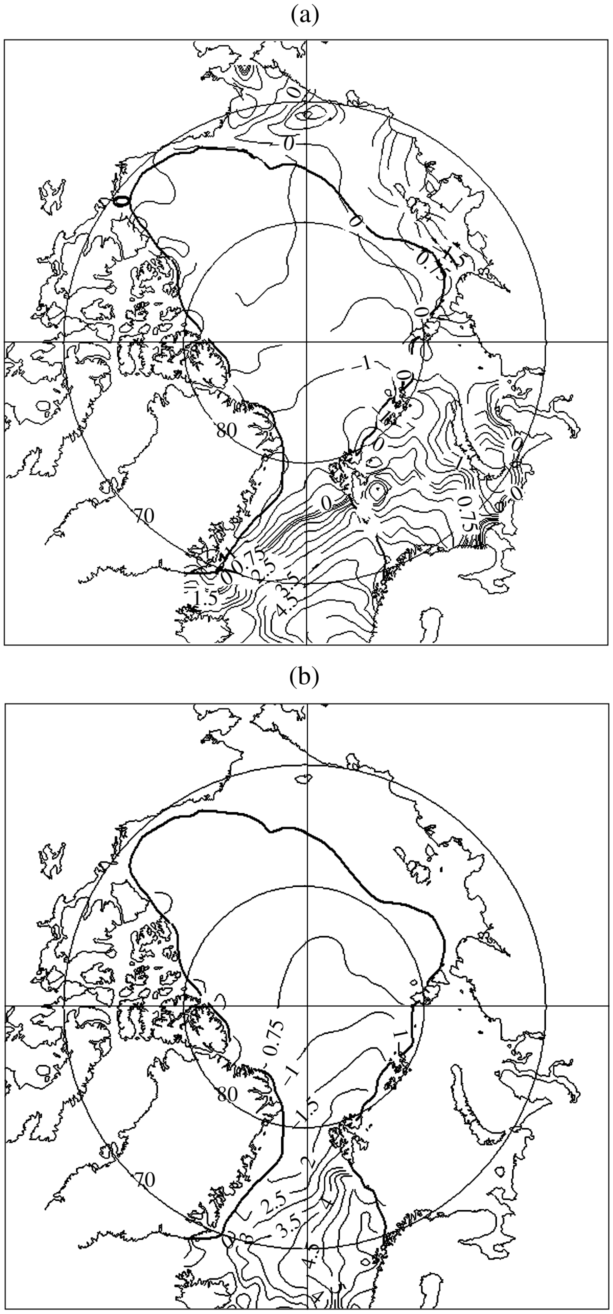

Fig. 5. Temperature (in °C) at a depth of (a) 50 m and (b) 400 m.

water on the Siberian shelf, which had apparently remained since the summer. One can clearly see the transport of warm waters from the Atlantic. In deeper layers, one can notice the tongue of warm Atlantic waters with a core at depths of 300–500 m (see Fig. 4b). At the same time, the penetration of warm Atlantic waters into the Central Arctic is insufficiently intense in comparison with the existing observational data: in the area of the Fram Strait, the aforementioned recirculation of warm waters in the north (coinciding in its position with the isotherm + 1°C) and cold waters in the south. Therefore, the reproduced tongue of warm waters is extremely wide. By the way, such a smoothed structure is typical of all models with a horizontal resolution of 40–100 km (see the results on the AOMIP site at http://fish.cims.nyu.edu/project_aomip/overview.html).

The annual cycles of the temperature and salinity fields can be traced up to a level of 50–100 m, except for the continental slope at the northern end of the Kara Sea, where the seasonal cycle is traced up to a depth of 300 m. By the way, it is this area that is characterized by high flow velocities on the continental slope (Fig. 4b).

In the salinity field on the ocean surface (Fig. 6), one can see a relatively freshwater Beaufort Sea with a salinity of about 29‰ in August and 30.5‰ in late winter in May, the advection (along the Alaska coast) of Pacific waters penetrating through the Bering Strait with a salinity of about 31‰ and transport of Atlantic waters through the Barents Sea with a salinity of more than 34‰. On the Siberian shelf, there is a clearly defined annual trend, which is caused by the flow of large Siberian rivers with fluctuations of minimum salinity from 17 to 25‰.

Such distributions of salinity seem quite realistic, although there are some problems with the description of the observed salinity in the Beaufort Sea and with the reproduction of the freshwater content both in the Beaufort Sea and in the Arctic Ocean as a whole.

5. CONCLUSIONS

It can be concluded that the coupled model of the Arctic Ocean water and sea-ice dynamics presented in this paper yields quite realistic results and is comparable to other state-of-the-art high-level models by its actual and potential capabilities. The model can be used within the frameworks of IPY 07–08 and the European contribution of DAMOCLES (http://www.damocles-eu.org) for assessing the role of tides in the formation of the Arctic Ocean climate and for assessing the sensitivity of the Arctic Ocean to changes in external forcings.

The aforementioned shortcomings in reproducing the observed state of the Arctic Ocean can be attributed partly to the flaws of the mathematical formulation of the problem, partly to the problems with accuracy and conformity of the atmospheric forcing being used (especially, this concerns cloudiness, humidity, and precipitation), partly to the low spatial resolution of the model, and, finally, to the problems of choosing adequate computational algorithms.

The mathematical formulation of the problem does not ensure the exact conservation for the salt mass and freshwater volume, and, consequently, the reproduction of ocean salinity (this can be seen by the salinity field in the Beaufort Sea). To eliminate this defect, it is necessary to reformulate the problem with allowance for the change in the volume of liquid water. Such a study is currently underway.

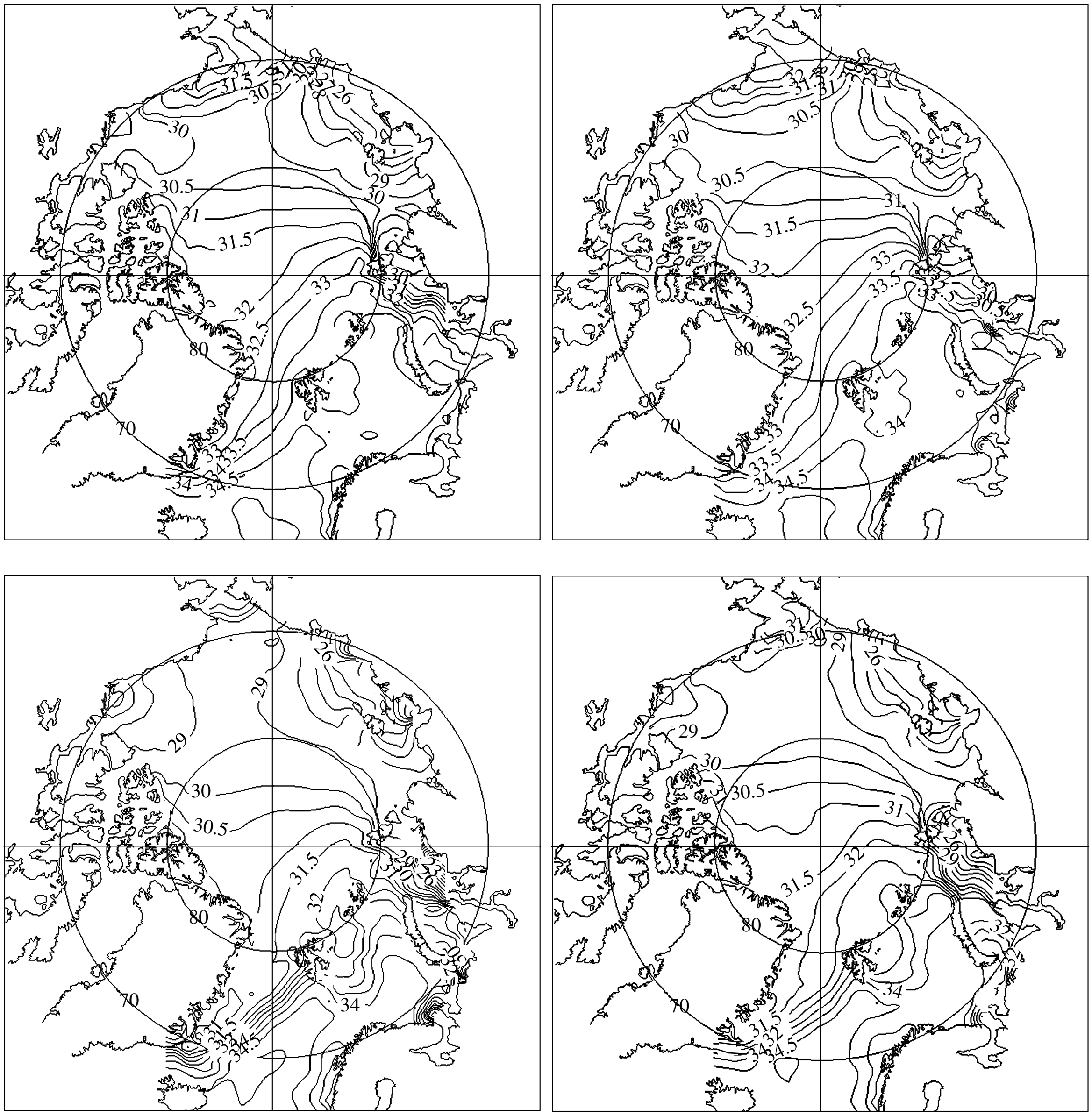

Fig. 6. Salinity on the ocean surface, ‰. Left to right and top to bottom: February, May, August, and November.

The hydrostatic approximation cannot describe such a process as the transport of dense shelf waters along the continental slope into the deep ocean as well as the penetration of bottom waters from one trough into another through faults in underwater ridges. This problem is solved by using so-called “quasi-physical” parametrizations such as [65, 66].

The low spatial resolution does not allow the mechanism of generation of narrow alongshore jets to be described explicitly. This problem can be partially solved with the help of a Neptune-effect type parametrization. However, this parametrization in principle will not yield the observed depth-inhomogeneous flow in the Fram Strait. This problem is partly solved by using a parametrization of the eddy transfer of a scalar. To simulate these transfers directly, it is probably necessary to resolve the first baroclinic Rossby radius (in the Arctic Ocean, this value is approximately a few kilometers). The same can be applied to the problem of enlargement of model-domain dimensions, which will ease the problem of boundary conditions in the straits connecting the Arctic Ocean with the Pacific and Atlantic oceans.

ACKNOWLEDGMENTS

This study was supported by the Russian Foundation for Basic Research, project nos. 03-05-64357 and 06-05-65225, and the European Commission project

DAMOCLES within the Sixth Framework Programme (FP6).

REFERENCES

1. A. Proshutinsky, M. Steele, J. Zhang, et al., "Multinational Effort Studies Differences among Arctic Ocean Models," EOS **82** (51), 637–644 (2001).
2. A. S. Sarkisyan, V. B. Zalesnyi, N. A. Dianskii, et al., "Mathematical Models of the Circulation of Oceans and Seas," in *Current Problems of Numerical Mathematics and Mathematical Modeling*, Vol. 2, *Mathematical Modeling* (Nauka, Moscow, 2005), pp. 176–278 [in Russian].
3. N. G. Yakovlev, "Coupled Model of Ocean General Circulation and Sea Ice Evolution in the Arctic Ocean," Izv. Akad. Nauk, Fiz. Atmos. Okeana **39**, 394–409 (2003) [Izv., Atmos. Ocean. Phys. **39**, 355–368 (2003).
4. N. G. Yakovlev, "Numerical Simulation of the Large-Scale Circulation of Waters and Sea Ice in the Arctic Ocean," in *Geography and Natural Resources: Special Issue: Proceedings of the Conference on Measurements, Modeling, and Information Systems for Environmental Studies ENVIROMIS-2004* (Moscow, 2004), pp. 277–283.
5. N. G. Yakovlev, "Numerical Model of the General Circulation of the Arctic Ocean. A New Version and Preliminary Calculation Results," Russ. J. Numer. Anal. Math. Model. **13**, 465–478 (1998).
6. P. Uotila, D. M. Holland, MaquedaM. A. Morales, et al., "An Energy-Diagnostics Intercomparison of Coupled Ice-Ocean Arctic Models," Ocean Model. **11** (1–2), 1–27 (2006).
7. C. A. Paulson and J. J. Simpson, "Irradiance Measurements in the Upper Ocean," J. Phys. Oceanogr. **7**, 952–956 (1977).
8. G. I. Marchuk, V. P. Kochergin, V. I. Klimok, et al., "Mathematical Modeling of the Surface Turbulence in the Ocean," Izv. Akad. Nauk SSSR, Fiz. Atmos. Okeana **12**, 841–849 (1976).
9. V. P. Kochergin, "Three-Dimensional Prognostic Models," in *Coastal Ocean Models*, Ed. by N. Heaps (AGU, Coastal and Estuarine Science, 1987), Vol. 4, pp. 841–849.
10. I. V. Polyakov, "Diagnostic Computations of the Arctic Ocean Currents and Sea Level Variations," Izv. Akad. Nauk, Fiz. Atmos. Okeana **32**, 690–703 (1996) [Izv., Atmos. Ocean. Phys. **32**, 637–649 (1996)].
11. Z. Kowalik and I. Polaykov, "Diurnal Tides over Kashevarov Bank, Okhotsk Sea," J. Geophys. Res. C **104**, 5361–5380 (1999).
12. G. Holloway, "Representing Topographic Stress for Large-Scale Ocean Models," J. Phys. Oceanogr. **22**, 1033–1046 (1992).
13. E. Kazantsev and Sommeria J. Verron, Subgrid-Scale Eddy Parametrization by Statistical Mechanics in a Barotropic Ocean Model, J. Phys. Oceanogr. **28**, 1017–1042 (1998).
14. I. Polyakov, "An Eddy Parameterization Based on Maximum Entropy Production with Application to Modeling of the Arctic Ocean Circulation," J. Phys. Oceanogr. **31**, 2255–2270 (2001).
15. W. J. Merryfield, G. Holloway, and A. E. Gargett, "A Global Ocean Model with Double-Diffusive Mixing," J. Phys. Oceanogr. **29**, 1124–1142 (1999).
16. P. R. Gent and J. C. McWilliams, "Isopycnal Mixing in Ocean Circulation Models," J. Phys. Oceanogr. **20**, 150–155 (1990).
17. M. H. Redi, "Oceanic Isopycnal Mixing by Coordinate Rotation," J. Phys. Oceanogr. **12**, 1154–1158 (1982).
18. S. M. Griffies, "The Gent-McWilliams Skew-Flux," J. Phys. Oceanogr. **28**, 831–841 (1998).
19. G. Danabasoglu and J. C. McWilliams, "Sensitivity of the Global Ocean Circulation to Parameterizations of Mesoscale Tracer Transports," J. Clim. **8**, 2967–2987 (1995).
20. W. G. Large, G. Danabasoglu, S. C. Doney, et al., "Sensitivity to Surface Forcing and Boundary Layer Mixing in a Global Ocean Model: Annual-Mean Climatology," J. Phys. Oceanogr. **27**, 2418–2447 (1997).
21. C. L. Parkinson and W. M. Washington, "A Large-Scale Numerical Model of Sea Ice," J. Geophys. Res. C **84**, 311–337 (1979).
22. C. M. Bitz, M. M. Holland, A. J. Weaver, et al., "Simulating the Ice-Thickness Distribution in a Coupled Climate Model," J. Geophys. Res. C **106**, 2441–2463 (2001).
23. V. R. Vrieglieb, S. M. Vitz, and T. S. Hunke, et al., *Description of the Community Climate System Model Version 2: Sea Ice Model* (National Center for Atmospheric Research, 2002). Available at <http://www.ccsm.ucar.edu/models/ice-csim4>
24. T. C. Grenfell and G. A. Maykut, "The Optical Properties of Ice and Snow in the Arctic Basin," J. Glaciol. **18**, 445–463 (1977).
25. E. E. Ebert and J. A. Curry, "An Intermediate One-Dimensional Thermodynamic Sea Ice Model for Investigating Ice–Atmosphere Interactions," J. Geophys. Res. C **98**, 10 085–10 109 (1993).
26. F. J. Millero, "Freezing Point of Sea Water," in *8th Report of the Joint Panel on Oceanographic Tables and Standards, UNESCO Technical Papers in Marine Sciences* (UNESCO, Paris, 1978), Vol. 28, Annex 6, pp. 29–35.
27. M. G. McPhee, "Turbulent Heat Flux in the Upper Ocean Under Ice," J. Geophys. Res. C **97**, 5365–5379 (1992).
28. M. G. McPhee, "Turblent Stress at the Ice/Ocean Interface and Bottom Surface Hydraulic Roughness during the SHEBA Drift," J. Geophys. Res. **107**, doi: 10.1029/2001JC000633, C8037 (2002).
29. G. L. Mellor and L. H. Kantha, "An Ice-Ocean Coupled Model," J. Geophys. Res. C **94**, 10 937–10 954 (1989).
30. C. M. Bitz and W. H. Limpscomb, "An Energy-Conserving Thermodynamic Model of Sea Ice," J. Geophys. Res. CF **104**, 15 669–15 677 (1999).
31. W. D. Hibler III, "Modeling a Variable Thickness Sea Ice Cover," Mon. Weather Rev. **108**, 1943–1973 (1980).
32. G. M. Flato and W. D. Hibler III, "Ridging and Stress in Modeling the Thickness Distribution of Arctic Sea Ice," J. Geophys. Res. C **100**, 18 611–18 626 (1995).
33. D. A. Rothrock, "The Energetics of the Plastic Deformation of Pack Ice by Ridging," J. Geophys. Res. **80**, 4514–4519 (1975).
34. W. D. Hibler III, "A Dynamic-Thermodynamic Sea Ice Model," J. Phys. Oceanogr. **9**, 815–846 (1979).

35. E. C. Hunke and J. K. Dukowicz, "An Elastic–Viscous–Plastic Model for Sea Ice Dynamics," J. Phys. Oceanogr. **27**, 1849–1867 (1997).

36. E. C. Hunke, "Viscous–Plastic Sea Ice Dynamics in the EVP Model: Linearization Issues," J. Comput. Phys. **170**, 18–38 (2001).

37. M. Kreyshner, M. Harder, P. Lemke, et al., "Results of the Sea Ice Model Intercomparison Project: Evaluation of Sea Ice Rheology Schemes for Use in Climate Simulations," J. Geophys. Res. C **105**, 11 299–11 320 (2000).

38. A. Y. Proshutinsky and M. A. Johnson, "Two Circulation Regimes of the Wind Driven Arctic Ocean," J. Geophys. Res. C **102**, 12 493–12 514 (1997).

39. N. Steiner, "Introduction of Variable Drag Coefficients Into Sea-Ice Models," Ann. Glaciol. **33**, 181–186 (2001).

40. D. A. Rothrock, J. Zhang, and Y. Yu, "The Arctic Ice Thickness Anomaly of the 1990s: a Consistent View from Observations and Models," J. Geophys. Res. C **108**, doi: 10.1029/2001JC001208, C3083 (2003).

41. T. J. R. Hughes and A. Brooks, "A Multi-Dimensional Upwind Scheme with No Crosswind Diffusion," in *Finite Element Method for Convection Dominated Flows*, Ed. by T. J. R. Hughes (AMD, ASME, New York, 1979), Vol. 34, pp. 19–35.

42. T. J. R. Hughes, "Recent Progress in the Development and Understanding of SUPG Methods with Special Reference to the Compressible Euler and Navier–Stokes Equations," Int. J. Numer. Methods Fluids **7**, 1261–1275 (1987).

43. O. C. Zienkiewicz and R. L. Taylor, *The Finite Element Method*, 5th Ed., Vol. 3, *Fluid Dynamics* (Butterworth and Heinemann, Oxford, 2000).

44. P. Marchesiello, J. C. McWilliams, and A. Shchepetkin, "Open Boundary Conditions for Long-Term Integration of Regional Oceanic Models," Ocean Model. **3**, 1–20 (2001).

45. E. Kalnay, et al., "The NCEP/NCAR 40-Year Reanalysis Project," Bull. Am. Meteorol. Soc. **77**, 437–470 (1996).

46. R. Kistler, E. Kalnay, W. Collins, et al., "The NCEP-NCAR 50-Year Reanalysis: Monthly Means CD-ROM and Documentation," Bull. Am. Meteorol. Soc. **82**, 247–267 (2001).

47. J. W. Zillman, "A Study of Some Aspects of the Radiation and Heat Budgets of the Southern Hemisphere Oceans," in *Meteorological Studies* (Bureau of Meteorology, Dept. of the Interior, Canberra, Australia, 1972), Vol. 26.

48. A. Rosati and K. Miyakoda, "A General-Circulation Model for Upper-Ocean Simulation," J. Phys. Oceanogr. **18**, 1601–1626 (1988).

49. A. P. Makshtas, *The Heat Budget of Arctic Ice in the Winter* (International Glaciological Society, Cambridge, 1991), No. CB2 1ER UK.

50. A. Gill, *Atmosphere–Ocean Dynamics* (Academic, New York, 1982; Mir, Moscow, 1986).

51. F. Roeske, "An Atlas of Surface Fluxes Based on the ECMWF Re-Analysis," in *A Climatological Dataset to Force Global Ocean General Circulation Models* (Max Planck-Institut fur Meteorologie, 2001), Vol. 323.

52. *Atlas of the Arctic*, Ed. by A. F. Treshnikov (GUGK, Moscow, 1985) [in Russian].

53. *Environmental Working Group (EWG), 2000: Joint U.S.– Russian Arctic Atlas: The Arctic Climatology Project: Arctic Meteorology and Climate Atlas [CD-ROM]* (Natl. Snow and Ice Data Center, Boulder, Colorado, 2000).

54. M. C. Serreze, M. P. Clark, and D. H. Bromwich, "Monitoring Precipitation over the Arctic Terrestrial Drainage System: Data Requirements, Shortcomings and Applications of Atmospheric Reanalysis," J. Hydrometeorol. **4**, 387–407 (2003).

55. D. Yang, "An Improved Precipitation Climatology for the Arctic Ocean," Geophys. Rev. Lett. **26**, 1625–1628 (1999).

56. P. P. Xie and P. A. Arkin, "Analyses of Global Monthly Precipitation Using Gauge Observations, Satellite Estimates, and Numerical Model Predictions," J. Clim. **9**, 840–858 (1996).

57. M. Steele, R. Morley, and W. Ermold, "PHC: A Global Ocean Hydrography with a High Quality Arctic Ocean," J. Clim. **14**, 2079–2087 (2001).

58. H. Melling, "Exchanges of Freshwater through the Shallow Straits of the North American Arctic," in *The Freshwater Budget of the Arctic Ocean*, Ed. by E. L. Lewis et al. (Kluwer, Dordrecht, 2000), pp. 479–502.

59. M. Prange, *Einfluss arktischer Sauaswasserquellen auf die Zirkulation im Nordmeer und im Nordatlantik in einem prognostischen Ozean-Meereis-Modell*, PhD Thesis (Univ. of Bremen, Bremen, 2002).

60. K. Aagaard and E. C. Carmack, "The Role of Sea Ice and Other Fresh Water in the Arctic Circulation," J. Geophys. Res. C **94**, 14 485–14 498 (1989).

61. W. Chapman and J. Walsh, "Recent Variations of Sea Ice and Air Temperature in High Latitudes," Bull. Amer. Meteorol. Soc. **74** (1) (1993).

62. P. Wadhams, "Sea Ice Thickness Changes and Their Relation to Climate," in *The Polar Oceans and Their Role in Shaping the Global Environment* (AGU, Washington, 1994). Geophysical Monograph, Vol. 85, pp. 337–361.

63. R. Colony and I. Rigor, "Arctic Ocean Buoy Data Program Report," (Natl. Snow and Ice Data Center, Boulder, Colorado, 1995), Applied Physics Laboratory Technical Memo APL-UW TM 10–91.

64. S. G. Warren, I. G. Rigorn, N. Untersteiner, et al., "Snow Depth on Arctic Sea Ice," J. Clim. **12**, 1814–1829 (1999).

65. A. Beckmann and R. Doescher, "A Method for Improved Representation of Dense Water Spreading over Topography in Geopotential-Coordinate Models," J. Phys. Oceanogr. **27**, 581–591 (1997).

66. J.-M. Campin and H. Goosse, "Parameterization of Density-Driven Downsloping Flow for a Coarse-Resolution Ocean Model in Z-Coordinate," Tellus A, No. 51, 412–430 (1999).